Can vortex generators reduce power losses of utility-scale wind turbines due to blade leading edge erosion?

Thomas Collin[1], Alessio Castorrini[2,1], Sanshodhan Shende[2], Alexander Meyer Forsting[3] and M. Sergio Campobasso[1]

[1]School of Engineering, Lancaster University, Lancaster, UK
[2]Sapienza University of Rome, Rome, I
[3]DTU Wind, Technical University of Denmark, Roskilde, DK

E-mail: m.s.campobasso@lancaster.ac.uk

Abstract. Vortex generators (VGs) improve the aerodynamic performance of airfoils by increasing the angle of attack at which stall occurs at the expense of a small increase in profile drag. This study explores the potential of VGs to reduce wind turbine power and energy losses due to blade leading edge erosion. A 22 MW turbine, with blades assumed to be affected by different levels of leading edge erosion, is considered. Erosion is considered over the outer blade region, featuring a 21% thick airfoil. The turbine performance from cut-in to cut-out wind speed is determined with turbulent aero-servo-elastic simulations. The curves of lift and drag coefficients of the outboard airfoil with and without erosion and with and without VGs are determined using Reynolds-averaged Navier-Stokes Computational Fluid Dynamics. Two offshore and one onshore sites are considered. VGs are found to start alleviating power and energy loss due to erosion only once erosion has reached advanced stages, corresponding to removal of the protective coating and initial damage of the composite substrate. For any given erosion level, the performance benefit of VGs is found to be more significant at the onshore site.

1. Introduction

Leading edge (LE) erosion of wind turbine (WT) blades has become a significant problem in the wind energy industry, due to both the cost of unplanned remedial maintenance, particularly high offshore, and the loss of Annual Energy Production (AEP) consequent to reduced aerodynamic performance of the blades.

Vortex generators (VGs) are passive flow control devices that can improve the aerodynamic performance of the airfoils of both fixed and rotating blades, such as those of rotorcraft and WTs [1]. Specifically, VGs delay stall, yielding higher lift and lower drag at the Angle of Attack (AoA) level at which the clean airfoil is already stalled. This performance enhancement comes at the cost of a small increase in the total drag in the region where neither the clean nor the VG-enhanced airfoil feature flow separation. In WT engineering, VGs are typically applied to the inboard part of the blades, where the AoA is close to or higher than the stall threshold. Thus, VGs reduce the occurrence of stall, reducing flow-induced vibrations and aerodynamic noise [2]. In modern multi-megawatt WTs, using rotor speed control before rated wind speed, and blade pitch-to-feather control above rated wind speed, the mean AoA values at the outboard

blade region are typically below the stall point over the entire operational range of mean wind speeds. However, the reduced stall margin due to severe LE erosion (LEE), together with large wind speed fluctuations due to atmospheric turbulence, may result in the blades operating for some time close to or in the stall region, with consequent power and AEP losses, and, potentially, increased fatigue due to stall-induced vibrations. Indeed, there is evidence that VGs are sometimes used also in the outboard blade region of modern multi-megawatt WTs [3], but limited literature on this application exists.

Placing VG pairs in the path of an incoming boundary layer (BL) yields the formation of two counter-rotating longitudinal vortices that transfer high-energy fluid of the bulk flow into the BL, reducing its thickness and improving its capability to withstand adverse pressure gradients without separating. The relationship between VG height and vortex strength was investigated with Computational Fluid Dynamics (CFD) and wind tunnel measurements in [4]. The study concluded that a VG height equal to the BL thickness offered the best trade-off between flow control effectiveness and profile drag increase. Skrzypiński *et al* [5] assessed the VG potential of reducing LEE-induced AEP losses of constant-speed and variable-pitch WTs. A 27-month experimental campaign was carried out and six WTs, three with and three without VGs, were monitored. The WTs with VGs showed an average increase in energy production of 3.3%.

This study aims to evaluate the potential of VGs fitted to the outboard blade portion to alleviate LEE-induced power and AEP losses of modern utility-scale WTs, which use variable speed and pitch control. The investigation employs CFD simulations of nominal and eroded blade sections with and without VGs, and WT turbulent aero-servo-elastic simulations.

2. Methodology

2.1. Selected wind turbine, outboard airfoil variants and VG geometry

The IEA Wind 22 MW reference WT [6] is used in this study. This direct-drive rotor speed- and blade pitch-controlled WT has rotor diameter of 284 m and hub height of 170 m. The cut-in, rated and cut-out speeds are, respectively, 3, 11 and 25 m/s. The rotor blades feature the 21% thick FFA-W3-211 airfoil from 98% rotor radius to the tip, and the 24% thick FFA-W3-241 airfoil at 74.7% rotor radius. The airfoils between 74.7 and 98% rotor radius are combinations of the two airfoils with radius-dependent weights. In this study, the outer blade shape has been slightly altered to reduce the number of CFD simulations: the FFA-W3-211 airfoil has been used from 70% blade length to the blade tip. The assumption does not significantly alter the findings of the analyses herein, as the curves of lift coefficient c_l and drag coefficient c_d versus AoA α of the 21% and 24% thick airfoils are very similar. The blades' internal structure has instead been kept unaltered. The nominal geometry of the FFA-W3-211 airfoil is plotted with a solid line in Fig. 1a.

Two levels of LEE are considered, a moderate and a severe one. Moderate corresponds to LE roughness due to partial erosion of the protective coating, whose nominal thickness varies between 1 and 2 mm. Severe LEE corresponds to the complete removal of the coating and initial erosion of the composite substrate.

The chord c of all models is 1 m and all geometric variables below refer to this reference length. The detrimental impact of moderate LEE on airfoil performance is accounted for by using a distributed roughness model [7, 8], considering a rough surface with equivalent sand grain roughness K_s =200 µm from x_l = 130 mm from the LE on the lower side to x_u = 50 mm from the LE on the upper side. The severe damage is geometrically resolved in the CFD simulations using an idealized chordwise groove model [9] with depth d = 1.5 mm and same curvilinear extension of the moderate damage. Distributed roughness with K_s =200 µm is also applied within the groove to account for the surface roughness of the eroded composite substrate.

The VG geometry is depicted in Fig. 1b. λ is the spanwise distance between two adjacent VG pairs, as well as the distance between the two periodic boundaries of the three-dimensional

(3D) CFD domain. The considered VG geometry, also referred to c=1 m, has $\lambda = 45$ mm, $S = 22.5$ mm, $l = 11.25$ mm, $H = 4.5$ mm and $\beta = 20°$.

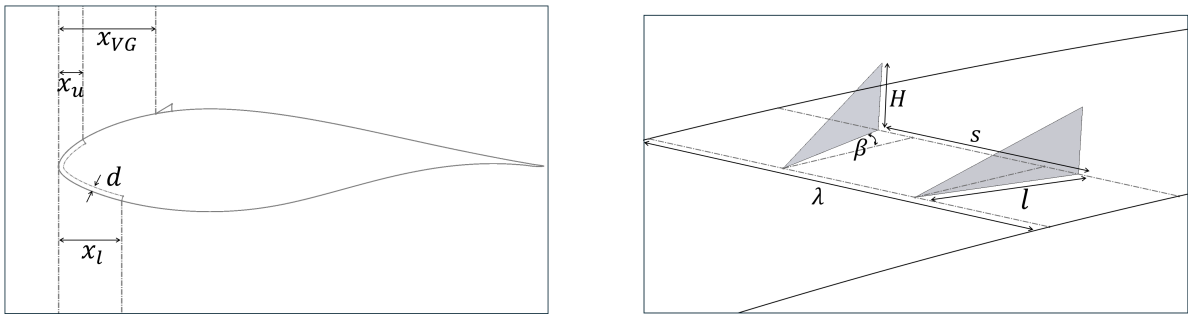

(a) (b)

Figure 1: (a): FFA-W3-211 airfoil with groove definition and VG position; (b) VG geometry.

2.2. CFD set-up

All analyses use the Reynolds-averaged Navier-Stokes (RANS) flow model. The incompressible solver of ANSYS Fluent version 2024 R2 is used in steady mode at all considered AoA values. The effects of turbulence on the mean flow are modeled with Menter's $k-\omega$ Shear Stress Transport (SST) model. Transitional BLs are simulated by means of the Langtry-Menter $\gamma - Re_\theta$ SST transition model.

Unless otherwise stated, all CFD results herein are computed at a Reynolds number Re of 10 million (M), and are obtained with 3D CFD simulations using polyhedral meshes with inflation layers at solid walls, generated with Fluent Meshing. All smooth-wall simulations integrate the differential equations of the $\gamma - Re_\theta$ SST model down to the wall; the adopted height of the grid cells adjacent to wall boundaries ensures that the nondimensionalized distance y^+ of the first cell centers off solid walls is smaller than 1 in all cases. The SST model with rough-wall functions is instead used for all analyses with distributed roughness. For each airfoil variant, simulations of the flow field from $-20°$ to $20°$ are performed. The distance of the far field boundary from the airfoil is 40 chords in all cases, as this value is the minimum one making the computed solution domain size independent. The four 3D simulation sets of the airfoil with smooth and rough surface with and without VGs use a common grid with 6,284,599 cells. The two 3D simulation sets of the grooved airfoil with and without VGs use a common grid with 6,956,777 cells. All 3D and two-dimensional (2D) simulations feature a freestream turbulence intensity (TI) of 0.1% and a turbulence length scale of 0.2 m. The constant a_1 of the $k-\omega$ SST model was set to 0.30 in all cases to improve stall predictions.

The number of iterations needed to achieve a residual drop of at least three orders of magnitude for the analyses of all six 3D simulation sets varies between 10,000 and 14,000.

In order to validate the adopted CFD set-up, the lift and drag curves of the smooth FFA-W3-211 airfoil at Re =6 M are computed with 2D simulations and compared to measurements at the same Re recently completed in the Poul la Cour wind tunnel at DTU Wind as part of the LERCat project [10]. The simulations use the same domain geometry and far field boundary conditions of the 3D simulation set-up reported above. The grid, generated with ANSYS Meshing, has fully structured topology and features 365,750 quadrilateral cells. Figure 2 highlights very good agreement of simulations and measurements for $-8° < \alpha < 12°$, but also an overprediction of the stall AoA, frequently observed when using eddy viscosity turbulence models.

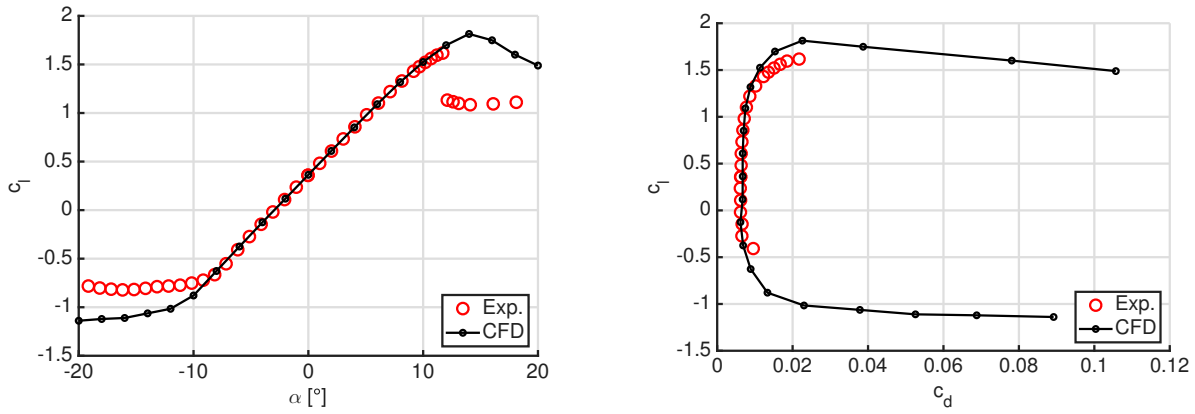

(a) c_l vs. AoA α. (b) Drag polar (c_l vs. c_d).

Figure 2: Computed and measured force coefficients of smooth FFA-W3-211 airfoil at $Re = 6$ M.

2.3. Sites and turbulent aero-servo-elastic analyses

An onshore site and two offshore sites are selected for the analysis of the power and AEP loss due to LEE and the variations of these metrics using VGs. The onshore site is Lancaster Hazelrigg in Northwest England, where a 2.3 MW is operational. The offshore sites are on the northeastern coast of Lampedusa island in the Mediterranean Sea, and a site in the North Sea (NS), off the western coast of Germany. Measured wind speed time-series with 10-min frequency over a one year period are available at all three sites. The coordinates of the three sites, the equipment used for the wind measurements and the methods to extrapolate the measured wind speed time-series at the hub height of 170 m of the WT considered herein are reported in [11]. Tab. 1 reports the scale factor c and the shape factor k of the three Weibull PDFs fitting the wind data extrapolated at hub height, along with the corresponding mean annual wind speed.

Table 1: Weibull PDF scale factor c and shape factor k, and hub height mean annual wind speed V_{mean} at selected sites. PDFs based on 10-min wind data bins at 170 m.

Site	c [m/s]	k [-]	V_{mean} [m/s]
Lancaster	8.21	1.89	7.3
Lampedusa	9.086	1.73	8.1
NS site	11.39	2.15	10.1

The aero-servo-elastic analyses of the WT with three FFA-W3-211 airfoil variants (nominal, moderately and severely eroded LE) without and with VGs, needed to determine power and AEP metrics, have been performed with OpenFAST version 4.1.0. Structural deformations have been resolved using the BeamDyn module, and maps of turbulent wind for each mean wind speed have been generated with the TurbSim code. The wind speed-dependent TI values used by TurbSim for the offshore sites (North Sea and Lampedusa) are those measured by the FINO1 met mast in the North Sea; the TI values used for the Lancaster site are those of the onshore wind of class B in the guidelines of the International Standard IEC61400. Further information on the adopted TI data is available in [8]. The shear exponents used by TurbSim for the offshore and onshore sites were 1/7 and 1/5, respectively. For the offshore simulations, the time step of OpenFAST was set to 2×10^{-4} s and the WT operation was considered for 3,000 s for each mean wind speed. For the onshore simulations, the time step of OpenFAST was set to 1×10^{-4} s and the WT operation was considered for 6,000 s. For all OpenFAST simulations, the mean value of all variables was calculated after removing the first 100 s of the analyses.

3. Results

3.1. Analyses of boundary layer thickness

The choice of the VG height was based on the estimated height range of the BL on the upper side of the smooth, and moderately and severely eroded airfoils at $0.2c$ for $5° < \alpha < 15°$. In order to compare the BL heights with the VG height of 4.5 mm, 2D CFD simulations of the three airfoil variants have been performed. The domain geometry, far field boundary conditions of these simulations without VGs are the same as those of the 3D simulations reported in Section 2.2. The grids, with a fully structured topology, are generated with ANSYS Meshing. That for the smooth and moderately eroded airfoils has 365,750 cells, and that for the severely eroded airfoil has 432,590 cells. The BL heights of the three airfoil variants are reported in Fig. 3. For given α, the BL thickness increases with the damage severity. The smallest thickness is that of the smooth airfoil for $0° < \alpha < 5°$, where the BL is still laminar. For $5° < \alpha < 15°$, the BL thickness of all three airfoils is comparable with the VG height, as desired.

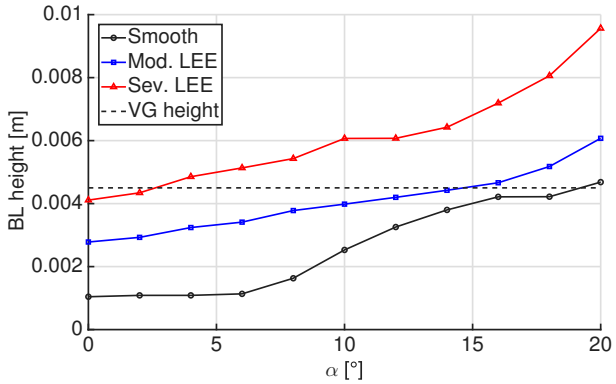

Figure 3: BL thickness at 20% chord on upper side of smooth, and moderately and severely eroded airfoils without VGs against AoA α at Re =10 M.

3.2. Airfoil aerodynamics with and without vortex generators

The $c_l - \alpha$ curves of the smooth, moderately and severely eroded FFA-W3-211 airfoils without and with VGs, all obtained with 3D CFD simulations, are compared in Fig. 4a. For all three airfoil variants, VGs increase the peak c_l value and the AoA at which it occurs. Without VGs, the stall angle decreases as LEE severity increases: it lies between 14° and 16° for the smooth airfoil, and drops to 12° for the severely eroded airfoil. The VG-enabled increase of the stall angle and the corresponding c_l depends on the LE state. VGs increase the maximum c_l of about 1.8 of the smooth airfoil to about 2.3, whereas they increase the maximum c_l of about 1.5 of the severely eroded airfoil to only about 1.7. Furthermore, visible VG-enabled c_l increases occur from $\alpha \approx 10°$ for the smooth airfoil, and from between 6° and 8° for the severely eroded airfoil. The differences possibly arise because, at these AoA levels, the BL thickness gets close to the VG height, as shown in Fig. 3. However, the investigation of the dependence of the VG benefit on the LE state requires additional analyses, *e.g.* comparing the shape factor H (ratio of BL displacement and momentum thickness) of the three airfoil variants. This is because increasing levels of LEE reduce the BL momentum [9], which is thus an additional key parameter in the design of VGs for eroded blades.

The drag polars of the six airfoil configurations in Fig. 4b indicate increasing drag levels in the linear region of the $c_l - \alpha$ curve as LEE increases. The values of c_d at $\alpha = 8°$ for the smooth, rough and grooved airfoils without VGs are, respectively, 0.010, 0.013 and 0.016. For given LEE level, VGs slightly increase c_d: at $\alpha = 8°$, the c_d values of the smooth, and moderately and

severely eroded airfoils with VGs are, respectively, 0.012, 0.015 and 0.017. However, for given LEE level, the use of VGs reduces significantly the profile drag above the stall angle of the airfoil without VGs, due to delayed stall. The curves of the ratio c_l/c_d against α are shown in Fig. 4c.

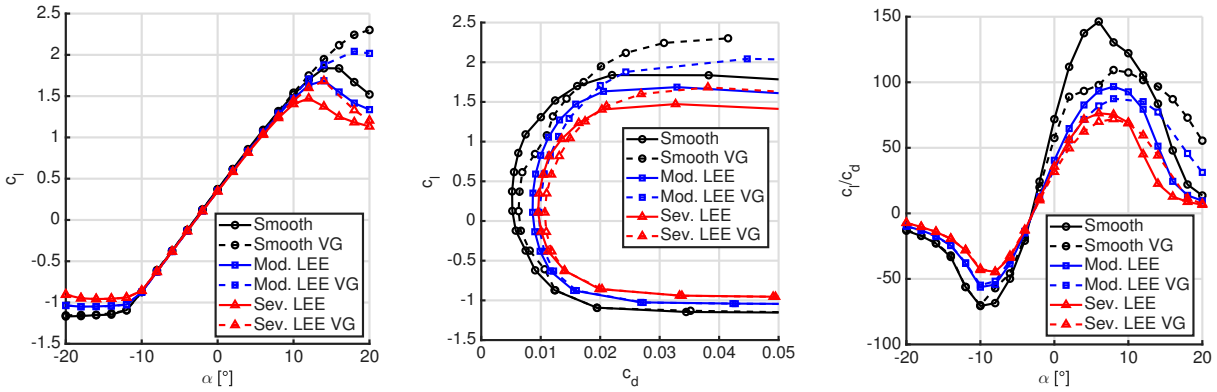

(a) c_l vs. AoA α. (b) Drag polar (c_l vs. c_d). (c) c_l/c_d vs. AoA α.

Figure 4: Force coefficients of smooth, and moderately and severely eroded FFA-W3-211 airfoil without and with VGs at Re =10 M.

The contours of the normalized velocity component parallel to the upper side of the smooth airfoil without VGs at $0.22c$, $0.33c$ and $0.44c$ from the LE for $\alpha = 14°$ are shown in the top plots of Fig. 5; the normalization is performed using the magnitude of the freestream velocity, and the width of all subplots equals the physical domain of the simulations; the counterpart of this sequence for the same airfoil with VGs is shown in the bottom plots. Cross-comparing the two plot sets highlights how the VG-induced vortices reduce the BL thickness. For example, the midspan BL height at $0.44c$ is 8.7 mm for the airfoil without VGs and 4.0 mm for that with VGs. The bottom left subplot also reports the projection of the VGs' rear edge on the planar section to help follow the BL evolution.

The contours of the normalized velocity component parallel to the upper side of the airfoil with severe LEE without VGs at $0.22c$, $0.33c$ and $0.44c$ for $\alpha = 12°$ are shown in the top plots of Fig. 6; the counterpart of this sequence for the airfoil with VGs is shown in the bottom plots. Also in this case, the VG-induced vortices reduce the BL thickness. The midspan BL height at $0.44c$ is 9.5 mm without VGs and 5.2 mm with VGs. Despite the AoA for the severely eroded airfoil analysis being lower than that for the smooth airfoil analysis, both BL heights are larger in the former case, due to the BL perturbation caused by the LE groove.

Figure 7 depicts the contours of vorticity magnitude of eight equally spaced planar sections on the upper side of the smooth and severely eroded airfoils with VGs at $\alpha = 10°$ and $\alpha = 14°$. Cross-comparing the smooth airfoil contour maps at the two AoA values points to slightly higher strength of the vortices at $\alpha = 14°$, particularly in the rear sections. This may be due to the BL thickness for $\alpha = 14°$ at the VG chordwise location being closer to the VG height than for $\alpha = 10°$, as shown in Fig. 3. Cross-comparing the vorticity maps of the smooth and severely eroded airfoils at $\alpha = 10°$ points to slightly higher vortex strength for the latter airfoil. This difference may arise because at $\alpha = 10°$ the BL thickness of the airfoil with severe LEE at the VG position exceeds the VG height, whereas that of the smooth airfoil is smaller; the overall lower momentum of the BL of the airfoil with severe LEE may also account for the highlighted difference. At $\alpha = 14°$, the vortices of the severely eroded airfoil are dissipated more rapidly due to the trailing edge separation.

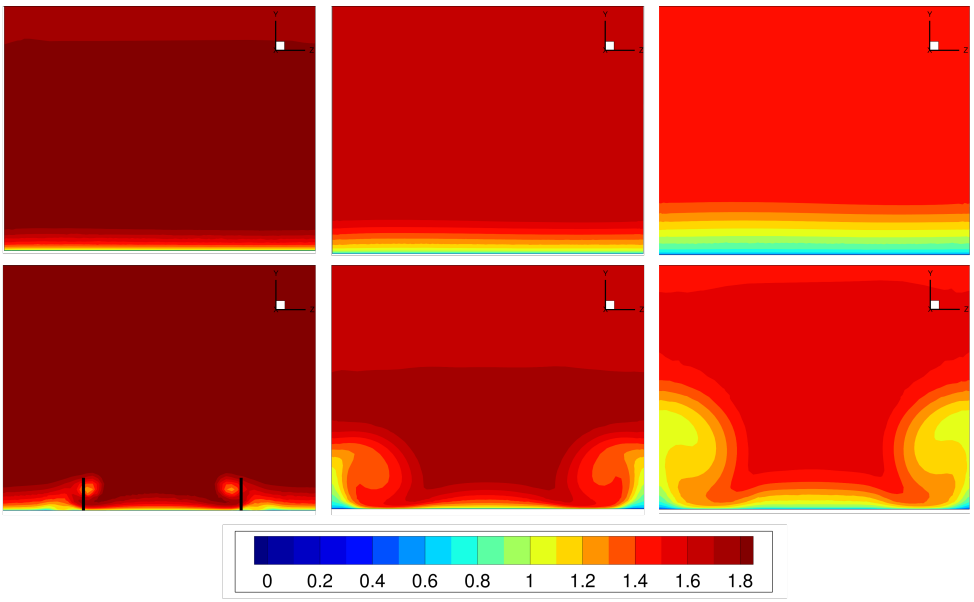

Figure 5: Contours of normalized velocity component parallel to upper side of smooth airfoil without VGs (top plots) and with VGs (bottom plots) at $\alpha = 14°$ in planar sections $0.22c$, $0.33c$ and $0.44c$ from LE.

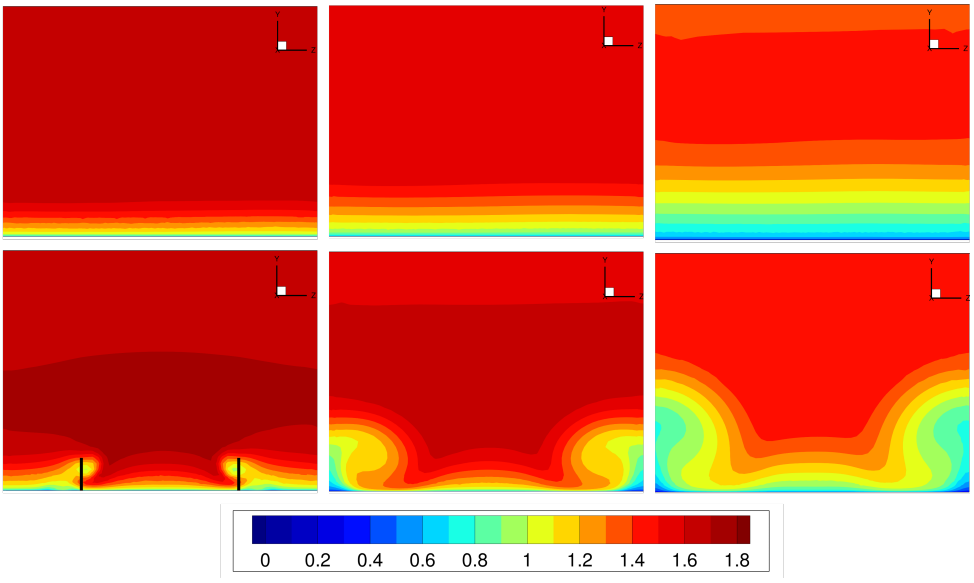

Figure 6: Contours of normalized velocity component parallel to upper side of severely eroded airfoil without VGs (top plots) and with VGs (bottom plots) at $\alpha = 12°$ in planar sections at $0.22c$, $0.33c$ and $0.44c$ from LE.

3.3. Comparative analyses of wind turbine performance

Figure 8 shows the power variations of the considered WT without and with VGs for the smooth, and moderately and severely eroded LE states. Figures 8a and 8b, in which V denotes the mean wind speed, refer to offshore and onshore turbulence levels, respectively. The power curve of the nominal WT ('Smooth') is to be read on the left axis, whereas the percentage power variation of the five WT variants (difference between power of the nominal WT and that of the considered

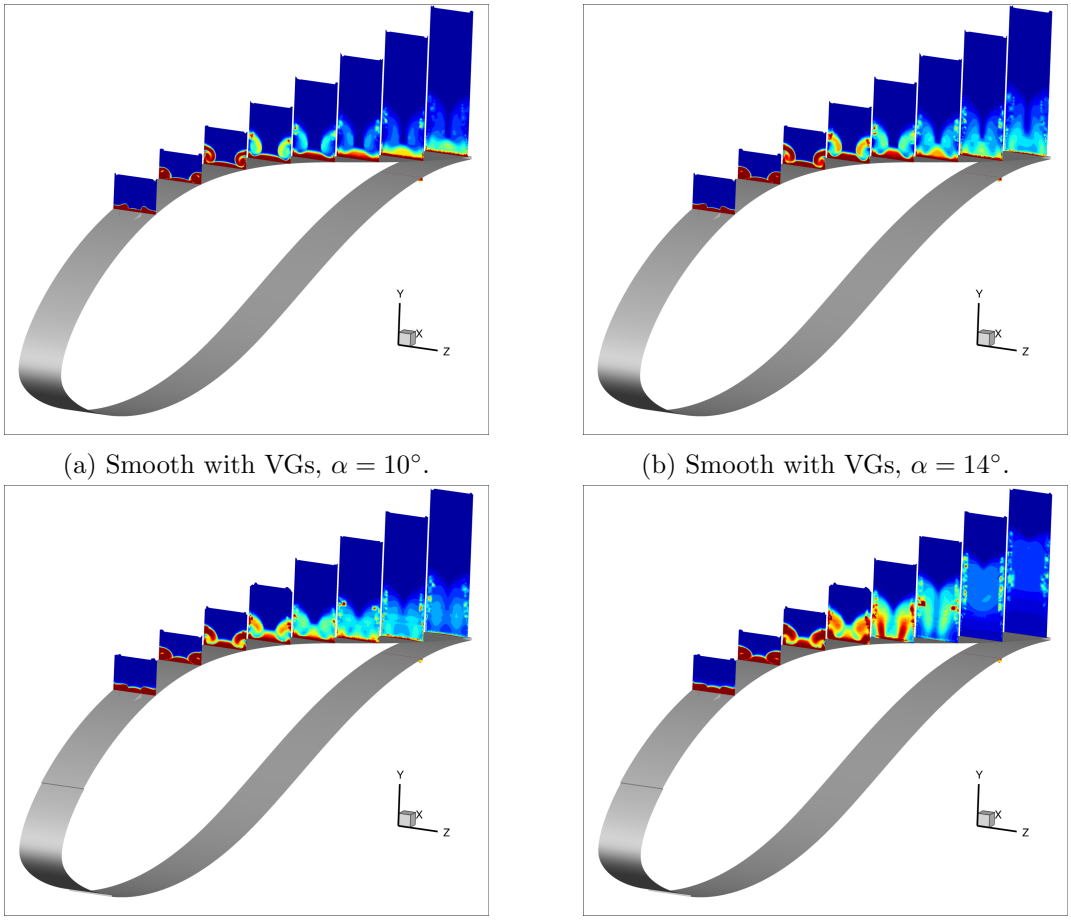

(a) Smooth with VGs, $\alpha = 10°$.

(b) Smooth with VGs, $\alpha = 14°$.

(c) Sev. LEE with VGs, $\alpha = 10°$.

(d) Sev. LEE with VGs, $\alpha = 14°$.

Figure 7: Contours of vorticity magnitude on eight equispaced sections on upper sides of smooth and severely eroded airfoils with VGs. Minimum and maximum vorticity levels are 0 and 10,000 [s^{-1}], respectively. First and eight sections are at $0.22c$ and $0.99c$, respectively.

variant, normalized by the power of the nominal WT) is reported on the right axis.

The data of Fig. 8a show that the use of VGs on the outer 30% of the blades of the nominal WT reduces power by about 0.5% at most V values below rated. VGs slightly increase power losses below rated speed also at moderate LEE: the percentage losses without and with VGs amount to about 1.5% and 1.8%, respectively. The AoA of the smooth and moderately eroded WT below 10 m/s is about 8°. As shown in Fig. 4, the c_l values with and without VGs are comparable at this AoA, but VGs increase profile drag. This leads to a torque reduction using VGs, which, for reasons linked to the WT control and discussed below, also slightly reduces the rotor speed. Conversely, VGs reduce the power loss due to severe LEE, increasingly as V decreases from 9 to 5 m/s; at the latter speed, the power losses without and with VGs are, respectively, 4.5% and 3.9%. This trend inversion can be explained by the pattern of the force coefficients of Fig. 4. With severe LEE, AOA values increase with respect to the nominal WT; consequently, the benefits of VGs also increase, since VGs yield c_l increases that outweigh c_d increases. For $8° < \alpha < 10°$, c_l increases from between 1.23 and 1.40 to between 1.25 and 1.45, whereas c_d increases by a more modest amount, from between 0.016 and 0.020 to between 0.017 and 0.021 (the VG-induced c_d increase for the smooth and moderately eroded airfoils is remarkably higher). These effects cause VGs to increase the torque and the rotation speed of

the severely eroded rotor, slightly reducing the power loss.

The power loss curves of Fig. 8b highlight that, at onshore turbulence level, LEE-induced power losses are higher than at the lower atmospheric turbulence of offshore operation, as reported in [9]. The results of Fig. 8b also point to higher effectiveness of the outboard blade VGs in reducing power losses due to LEE. This is because the larger velocity fluctuations onshore increase the time spent by the blade at higher AoAs, where VG-enabled performance improvements are larger.

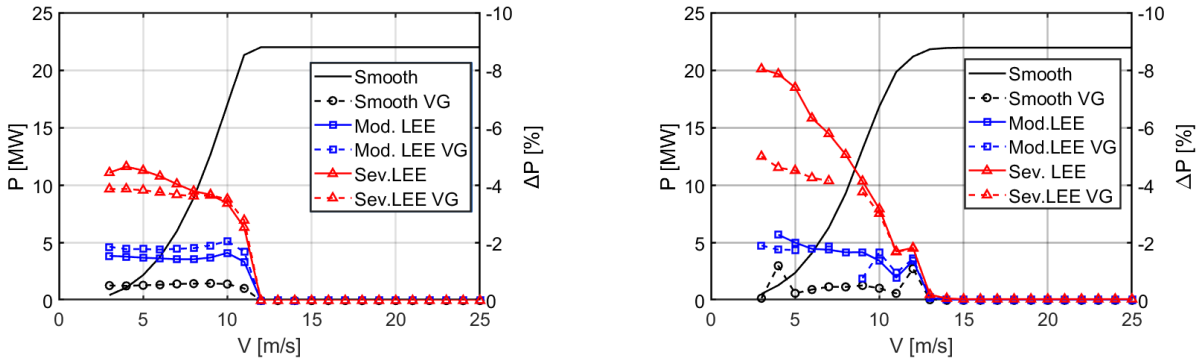

(a) Offshore turbulence level.

(b) Onshore turbulence level.

Figure 8: Power curve of nominal WT (solid black line, read on left axis) and power loss curves of nominal WT with VGs and eroded variants without and with VGs (read on right axis).

Figure 9 reports the mean AoA α along the blade of the nominal WT and the mean AoA variation $\Delta\alpha$ for the other five WTs relative to the nominal WT at V=10 m/s and V=5 m/s offshore. Without VGs, AoA values slightly increase with LEE severity at both 10 and 5 m/s, particularly where LEE occurs. This is partly because the speed controller uses a quadratic law between rotor torque and speed, with a coefficient of proportionality depending on the maximum power coefficient $C_{P,max}$ and the corresponding optimal tip-speed ratio $\lambda_{T,opt}$, to set the rotor speed. Since the control is unaware of the LEE-induced $C_{P,max}$ and $\lambda_{T,opt}$ variations, the reduced torque of the eroded WT also reduces the rotor speed; thus, for given V, AoA values increase. This rotor speed reduction was also reported in [12].

With moderate LEE at 10 m/s, VGs strengthen these effects, because AoA values are well below the stall threshold: the lift without and with VGs is comparable and the drag increase with VGs prevails (the same occurs with VGs fitted to the smooth blade). With severe LEE, however, the eroded blade portion without VGs moves further towards stall: the profile drag difference without and with VGs decreases and the VG-enabled lift increase is more pronounced. Thus, rotor torque and speed without and with VGs are closer than they are with moderate LEE. Hence, the $\Delta\alpha$ curves of the severely eroded blade without and with VGs in Fig. 9a are closer. Correspondingly, the power loss of the severely eroded WT without and with VGs is comparable. At V=5 m/s (Fig. 9b), AoA levels increase due to lower tip-speed ratio in the control schedule. Thus, the benefit of VGs on the eroded blades also increases, yielding relatively larger torque and rotor speed increases and, thus, reduced power losses. Fig. 9b highlights the VG-induced AoA reduction of the severely eroded blade due to higher rotor torque and speed.

WT performance reductions following VG installation were also mentioned in [13], which may underline the importance of tuning the speed control. In this regard, the use of adaptive rotor speed control [14], whereby the control is tuned to account for variations of the $\lambda_{T,opt}$ and $C_{P,max}$ due to both LEE and VGs, may further improve the VG benefits on the power output of WT affected by LEE.

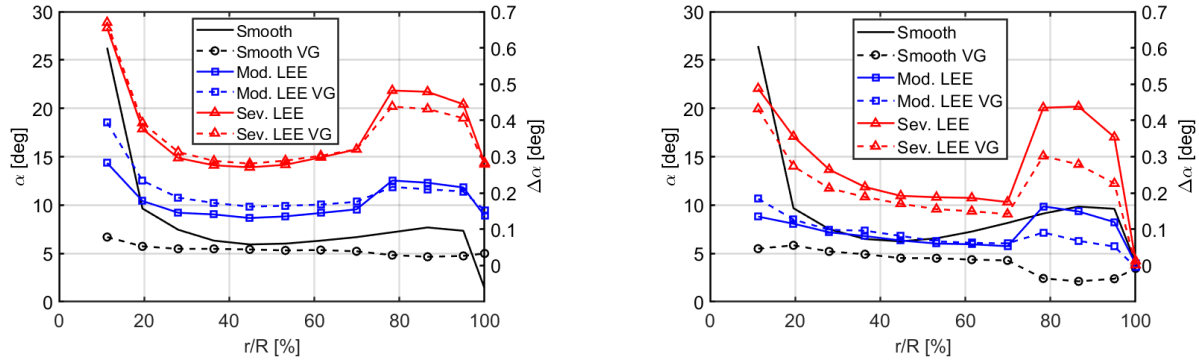

(a) V=10 m/s. (b) V=5 m/s.

Figure 9: Radial profile of AoA of nominal WT (solid black curve, read on left axis), and AoA variations of nominal WT with VGs and eroded variants with and without VGs (read on right axis) at offshore turbulence level.

Table 2 reports the AEP of the nominal WT and the percentage AEP losses of the nominal WT with VGs, and the eroded WTs without and with VGs at the three sites. The power curves of Fig. 8a are used for the Lampedusa and NS sites, and those of Fig. 8b for the Lancaster site. For given WT variant, AEP losses are always higher at the onshore site, due to both higher atmospheric turbulence and lower mean annual speed, as discussed in [9]. The impact of VGs on AEP losses is qualitatively similar onshore and offshore. In both cases, VGs reduce the loss due to severe LEE, but the reduction is notably higher onshore, since VGs may improve WT performance only below rated wind speed (above rated, the pitch control makes generated power insensitive to blade geometry alterations) and the mean wind speed at the onshore site is lower than at the offshore sites. For the nominal and moderately eroded WTs, VGs are found to increase AEP losses both offshore and onshore, in line with the power curves of Fig. 8.

Table 2: AEP of nominal WT and percentage AEP losses of WT variants at considered sites.

Site	Nominal AEP [MWh]	AEP Loss (%)				
		Smooth VG	Mod. LEE –	Mod. LEE VG	Sev. LEE –	Sev. LEE VG
Lancaster	68115	0.39	1.11	1.37	2.97	2.42
Lampedusa	78875	0.28	0.77	0.97	1.84	1.81
NS	109369	0.23	0.64	0.80	1.48	1.47

4. Conclusions

This CFD study finds that the effectiveness of VGs on the outer 30% of the blades of the IEA 22 MW WT in reducing LEE-induced power and AEP losses increases with LEE severity and site turbulence, and decreases with the site mean annual wind speed. Specifically, VGs reduce the AEP loss due to severe LEE at both the offshore and onshore sites considered, with the loss dropping from 2.97 to 2.42% at the onshore site, and decreasing notably less at the offshore sites. VGs always reduce the power of the WTs with nominal and moderately eroded blades.

The VG performance may be improved by tuning the speed controller, accounting for the $\lambda_{T,opt}$ and $C_{P,max}$ variations due to blade aerodynamics alterations with LEE and VGs.

The VG geometry and position were not optimized, but it is unlikely that this would significantly improve the performance of the VG-fitted WTs of this study, because the design

AoA of the nominal outboard blade region is well below the CFD-predicted stall point. Large LE perturbations are needed for the VG performance enhancement to become active. Thus, the benefit of retrofitting VGs to improve power and AEP is nominal blade-design dependent.

Lastly, it is noted that: 1) real-world severe LEE may reduce blade performance more than the idealized 2D pattern herein; 2) RANS CFD overestimates the stall AoA of the nominal airfoil. Both factors may results in the VG effectiveness being higher than reported herein.

Acknowledgments
This research was supported by the UK Engineering and Physical Sciences Research Council, Grant EP/W524438/1, and the Italian "Ministero dell'Ambiente e della Sicurezza Energetica", Grant "RdS PTR 2025-2027 - Energia dal mare". All CFD simulations were performed on Lancaster University's HEC cluster. The wind tunnel data of the FFA-W3-211 airfoil were produced in the LERCat project funded by the Danish Energy Council (EUDP-64021-2027).

References

[1] Sørensen N N *et al.* 2014 Prediction of the Effect of Vortex Generators on Airfoil Performance *Journal of Physics: Conference Series* **524** 012019

[2] Zhao Z *et al.* 2022 Researches on vortex generators applied to wind turbines: A review *Ocean Engineering* **253** 111266

[3] Mayda E *et al.* 2013 Wind Turbine Rotor R&D – an OEM Perspective international Conference on Future Technologies for Wind Energy. University of Wyoming, USA

[4] Li X *et al.* 2019 Experimental and Numerical Analysis of the Effect of Vortex Generator Height on Vortex Characteristics and Airfoil Aerodynamic Performance *Energies* **12**

[5] Skrzypiński W *et al.* 2020 Increase in the annual energy production due to a retrofit of vortex generators on blades *Wind Energy* **23** 617–626

[6] Zahle F *et al.* 2024 Definition of the IEA Wind 22-Megawatt Offshore Reference Wind Turbine Tech. Rep. E-0243 DTU Wind, Technical University of Denmark Roskilde,Denmark

[7] Campobasso M *et al.* 2022 Experimentally validated three-dimensional computational aerodynamics of wind turbine blade sections featuring leading edge erosion cavities *Wind Energy* **25** 168–189

[8] Castorrini A *et al.* 2023 Assessing the progression of wind turbine energy yield losses due to blade erosion by resolving damage geometries from lab tests and field observations *Renewable Energy* **218** 119256

[9] Campobasso M S *et al.* 2023 Probabilistic analysis of wind turbine performance degradation due to blade erosion accounting for uncertainty of damage geometry *Renewable and Sustainable Energy Reviews* **178** 113254

[10] Olsen A *et al.* 2026 Aerofoil performance degradation due to realistic leading edge roughness Paper under review Torque conference, Bruges, Belgium

[11] Campobasso M S *et al.* 2026 Development, performance and energy trade-off analyses of wind turbine precipitation-reactive control at offshore and onshore sites in western europe *Renewable Energy* **262** 125357

[12] Cappugi L *et al.* 2021 Machine learning-enabled prediction of wind turbine energy yield losses due to general blade leading edge erosion *Energy Convers Manag* **245** 114567

[13] Malik T H and Bak C 2024 Full-scale wind turbine performance assessment using the turbine performance integral (TPI) method: a study of aerodynamic degradation and operational influences *Wind Energy Science* **9** 2017–2037

[14] Campobasso M *et al.* 2020 Rapid Estimate of Wind Turbine Energy Loss due to Blade Leading Edge Delamination Using Artificial Neural Networks *J Turbomach* **142**